

## Does AMSR2 produce better soil moisture retrievals than AMSR-E over Australia?

Eunsang Cho <sup>a</sup>, Chun-Hsu Su <sup>b</sup>, Dongryeol Ryu <sup>b</sup>, Hyunglok Kim <sup>c</sup>, Minha Choi <sup>c,\*</sup>

<sup>a</sup> Department of Civil and Environmental Engineering, University of New Hampshire, Durham, NH, USA

<sup>b</sup> Department of Infrastructure Engineering, The University of Melbourne, Parkville, Victoria, Australia

<sup>c</sup> Water Resources and Remote Sensing Laboratory, Department of Water Resources, Graduate School of Water Resources, Sungkyunkwan University, Suwon 440-746, Republic of Korea



### ARTICLE INFO

#### Article history:

Received 2 October 2015

Received in revised form 14 October 2016

Accepted 30 October 2016

Available online xxxx

#### Keywords:

Remotely sensed soil moisture

Microwave sensor

AMSR2

AMSR-E

MERRA-L

Evaluation

Error estimation

### ABSTRACT

The Advanced Microwave Scanning Radiometer 2 (AMSR2), a follow-up microwave sensor to the AMSR for Earth Observing System (AMSR-E), was launched on the Global Change Observation Mission 1 – Water (GCOM-W1) satellite in May 2012. It is as yet unclear if instrumental improvements in AMSR2 over AMSR-E have led to better soil moisture (SM) estimates, especially since there is no overlapping period of data between the sensors. This study focuses on comparing the results of AMSR2 and AMSR-E SM over Australia, distinguishing four Köppen climate zones to determine if AMSR2 is better than AMSR-E. This is achieved by selecting two year-long comparative time periods from the operating periods of AMSR-E and AMSR2, based on their statistical similarities in modeled SM as a proxy, using Modern Era Retrospective-analysis for Research and Applications-Land (MERRA-L). The AMSR2 and AMSR-E C- and X-band SM derived from the Land Parameter Retrieval Model (LPRM) was evaluated. Both AMSR2 C- and X-band SM products were found to show similar temporal patterns and spatial agreement with AMSR-E C- and X-band SM, supported by unbiased root mean square difference (ubRMSD) and R-values with MERRA-L SM, respectively. Using lag-based instrumental variable analysis to estimate the random error component of SM retrievals, the noise-to-signal ratios in AMSR2 X-band SM were found to be slightly higher than their AMSR-E counterparts. The improvements in AMSR2, such as the superior radiometric sensitivity and spatial resolution, have therefore not led to statistically significant differences in performance for LPRM retrievals at  $1/2^\circ \times 1/2^\circ$  grid resolution, when compared with AMSR-E. However, similarities in the metrics for AMSR2 and AMSR-E SM suggest that AMSR2 provides a valuable continuation to AMSR-E.

© 2016 Elsevier Inc. All rights reserved.

## 1. Introduction

Space-borne microwave remote sensors have provided the most practical means of monitoring the spatial variability of soil moisture (SM) in the global hydrologic cycle and understanding hydrological and meteorological processes over a diverse range of land surface conditions (Schmugge et al., 2002). Among these sensors, the Advanced Microwave Scanning Radiometer for Earth Observing System (AMSR-E) sensor onboard the Aqua satellite provided valuable SM observations between June 2002 and October 2011 (Njoku et al., 2003). The AMSR-E ceased normal operation on October 2011, due to a problem with the mechanical scanning of its antenna, and was replaced by the Advanced Microwave Scanning Radiometer 2 (AMSR2) launched on the Global Change Observation Mission 1 – Water (GCOM-W1) satellite (Okuyama and Imaoka, 2015). With a similar design to AMSR-E, the

AMSR2 sensor continues the AMSR-E measurements from May 2012. Compared to AMSR-E, AMSR2 has an improved calibration system, a larger passive microwave antenna to achieve better spatial resolution, and better radiometric sensitivity with 12-bit quantization. Also, AMSR2 has a C-band frequency (7.3 GHz) channel in addition to the original C-band frequency (6.9 GHz) to mitigate radio-frequency interference (RFI) effects that the original C-band frequency (6.9 GHz) experienced in certain regions (Njoku et al., 2005).

The AMSR-E SM products have been used in a wide range of applications: hydrological modeling (Brocca et al., 2010; Wanders et al., 2014, Alvarez-Garreton et al., 2015), landslide risk mapping (Ray et al., 2010), agricultural drought monitoring crop production decision support (Bolten et al., 2009, 2010) and drought index (Choi et al., 2013), land surface modeling for root-zone SM estimation (Draper et al., 2012), rainfall estimation (Crow et al., 2011), and the construction of long-term climate records of soil moisture (de Jeu et al., 2012; Wagner et al., 2012). It is also expected that passive microwave products can be used in the study of energy balance modeling (Crow & Wood, 2002), land-atmosphere coupling (Miralles et al., 2014; Jung et al., 2010), and ecohydrology (Turner et al., 2003). These applications

\* Corresponding author at: Department of Water Resources, Graduate School of Water Resources, Sungkyunkwan University, Suwon 440-746, Republic of Korea.

E-mail addresses: [ec1072@wildcats.unh.edu](mailto:ec1072@wildcats.unh.edu) (E. Cho), [cusu@unimelb.edu.au](mailto:cusu@unimelb.edu.au) (C.-H. Su), [dryu@unimelb.edu.au](mailto:dryu@unimelb.edu.au) (D. Ryu), [hlkim@skku.edu](mailto:hlkim@skku.edu) (H. Kim), [mhchoi@skku.edu](mailto:mhchoi@skku.edu) (M. Choi).

could be tested with AMSR-E data owing to its long data record and its extensive validation (e.g., Champagne et al., 2010; Cho et al., 2015b; Draper et al., 2009; Gruhier et al., 2010; Jackson et al., 2010; Rossato et al., 2011; Su et al., 2013a, 2013b; Zeng et al., 2015). Given their instrumental similarities, the applications of AMSR2 are expected to be closely related to the existing and future studies involving AMSR-E. As the data stream of AMSR-E is now continued by AMSR2, it is necessary to ask how the research studies with AMSR-E SM can be interpreted in relation to the new instrument. Further, how do instrumental improvements to the microwave radiometer translate into improvements in the retrieved SM data? There exists a known issue of a maximum calibration difference up to 5 K collected by AMSR2, compared to other existing microwave satellite sensors (Tropical Rainfall Measuring Mission Microwave Imager (TMI) and AMSR-E) with similar instrument specifications (Okuyama and Imaoka, 2015). Although some possible reasons for these differences, including the reflector loss and receiver non-linearity, have been suggested by Okuyama and Imaoka (2015) and Imaoka et al. (2010), investigation of the underlying causes is still underway, and consequently the influence of the calibration differences on retrieved SM estimates remains uncertain. As the differences in Tb are somewhat unknown between the two sensors, a check of the consistency between the SM datasets could help understand the Tb issues better. Within this context, an alternative goal is to quantify the relative quality or errors between the SM products derived from the two instruments using same SM retrieval algorithm. This is the focus of our study. This approach is distinct from the recent studies by various authors, including Kim et al. (2015), who compared two AMSR2 X-band products created by the Japan Aerospace Exploration Agency (JAXA) algorithm and the Land Parameter Retrieval Model (LPRM) developed by the VU University Amsterdam with the National Aeronautics and Space Administration (NASA), Cho et al. (2015a) who evaluated AMSR2 SM using in situ measurements over the Korean peninsula, and Parinussa et al. (2015) who related the differences between AMSR-E and AMSR2 observed brightness temperature to different calibration procedures and small differences in sensor specifications.

This work focuses on comparison between AMSR-E and AMSR2-retrieved SM products derived by the Land Parameter Retrieval Model (LPRM) (Owe et al., 2008; Parinussa et al., 2015), although readers are referred to a recent review by Mladenova et al. (2014) for alternative retrieval algorithms. The LPRM algorithm, which is based on a forward radiative transfer model, uses both horizontal and vertical polarization of the C- or X-band observations to retrieve surface SM, and the Ka-band vertical polarized observation for the land surface temperature estimation. The LPRM delivers two products based on the C- (6.9 GHz) and X- (10.7 GHz) bands from AMSR-E, compared to three products from AMSR2, owing to the additional C-band (7.3 GHz) channel. This algorithmic consistency allows products derived from individual bands to be compared separately in this work. However, direct spatiotemporal point-to-point comparisons between AMSR-E and AMSR2 SM are not possible without temporal overlap between the two sensors. In order to overcome this obstacle, we propose the use of model-simulated SM as a proxy to identify periods during which the SM dynamics are statistically indistinguishable. The model SM dataset from NASA's MERRA-L (Modern Era Retrospective-analysis for Research and Applications-Land) re-analysis (Reichle et al., 2011) is used for this purpose. MERRA-L SM data are suitable due to remarkable performance globally in comparison with other reanalysis products (Albergel et al., 2013b; Al-Yaari et al., 2014; Yi et al., 2011). Section 2.2 describes the use of MERRA-L SM in this work more details.

Our study focuses on the entire Australian continent, in order to increase the statistical power of our analyses, but considers four Köppen climate zones separately: temperate with dry summer (denoted by Te-D hereafter), arid (Ard), tropical (Trp), and temperate without dry summer (Te-ND). Australia has complete coverage of high-quality microwave data where it is almost unaffected by RFI (Njoku et al., 2003). At the same time, the region provides several distinctive climate zones

and land surface characteristics to enable researchers to evaluate remotely sensed SM products over clearly classified spatial conditions. The differences between satellite and model SM are firstly examined during these statistically similar time periods, using conventional metrics. Subsequently, the random errors in individual SM products are estimated and compared using the lagged-variable (LV) instrumental variable analysis of Su et al. (2014a).

The paper is organized as follows. Section 2 describes the satellite and model SM datasets used in this work, as well as their pre-processing. The temporal sampling of satellite data for comparisons across the four climatic zones of Australia are presented in Section 3.1. Section 3.2 reviews the LV error estimation method. Section 4 details the results of our comparative analyses between satellite and modeled SM, and between AMSR-E and AMSR2 products. Finally, Section 5 offers our concluding remarks.

## 2. Data and pre-processing

### 2.1. AMSR2 and AMSR-E soil moisture

The AMSR2 is the follow-on instrument to AMSR-E (Imaoka et al., 2010). The main improvements of AMSR2 over AMSR-E are: a larger antenna, 2.0 m diameter compared to 1.6 m for AMSR-E; an additional channel in the C-band (7.3 GHz) to mitigate RFI; an improved calibration system; and additional momentum wheel (Okuyama and Imaoka, 2015). As a part of the Afternoon-train (A-train) constellation of satellites, AMSR2 has provided daily scans at approximately 1:30 a.m./p.m. (descending/ascending) local time at 1–2 days revisit time from May 2012 to the present day. There are two prominent AMSR2 SM products, namely the JAXA (Japan Aerospace Exploration Agency) (Koike, 2013) and NASA-VUA (VU University Amsterdam) LPRM products (Owe et al., 2008). Their X-band, Level 3 gridded products have been previously evaluated by Kim et al. (2015) against in situ measurements and it was found that the performances of both products decrease in usefulness under low mean temperature, dense vegetation, highly wetted conditions. The JAXA product shows better performance under dry conditions in terms of root-mean-square errors (RMSE) and biases, but the LPRM product has lower overall RMSE and biases (Kim et al., 2015). As our focus lies in distinguishing the influence of instrumental differences between AMSR-E and AMSR2 on SM retrievals, the LPRM products are used in this study. The LPRM algorithm uses the instrument's dual-polarization observations at individual (C or X) bands to simultaneously estimate the optical thickness of vegetation and the soil dielectric constant via the inversion of the microwave radiative transfer model. Also, the Ka-band (36.5 GHz) observations are used to estimate soil temperature. The LPRM then uses the dielectric mixing model of Wang and Schmugge (1980) to relate soil dielectric constant to volumetric SM in units of  $\text{m}^3 \text{m}^{-3}$ . Controlled by the observing wavelengths, the characteristic soil layer depths vary from <5 mm for the X-band and 1–2 cm for the C-bands. The LPRM uses a simplified land surface parameterization by assuming constant vegetation scattering albedo, surface roughness, and polarization mixing.

The AMSR2 LPRM, half-daily, Level 3 gridded, C1-(6.9 GHz), C2-(7.3 GHz), and X-(10.7 GHz) band SM datasets are provided on a regular  $1/4^\circ \times 1/4^\circ$  (latitude  $\times$  longitude) spatial grid. We used the most recent LPRM AMSR2 SM data set provided directly by Dr. Parinussa, which was generated from the re-calibrated brightness temperature data from JAXA. This product differs from the LPRM V001 product currently available from NASA GES DISC (Goddard Earth Sciences Data and Information Services Center), where its C1- and C2-band retrieved product show unusual temporal dynamics and significant positive bias, there are distinctive from AMSR-E, AMSR2 X-band and MERRA-L (Appendix B). In this study, AMSR2 was spatially upscaled to a  $1/2^\circ \times 1/2^\circ$  grid, by taking equal-weighted averages of their intra-grid values. The descending (1:30 a.m.) SM data is focus of our analyses as the LPRM is suited for the descending retrievals (Lei et al., 2015). For completeness, the

results for the ascending retrievals are presented in Appendix C (Figs. C1 and C2). In order to conduct paired comparisons between AMSR-E and AMSR2 SM, was mainly focused on the 6.9 GHz (C1-band, hereafter referred to as AMSR2 C-band) and 10.7 (X-band) products, such that the AMSR2 7.3 GHz (C2-band) product is excluded from our discussions in Sections 4.1 and 4.2, with the exception for Fig. 2.

The AMSR-E sensor on the Aqua satellite was similarly placed in the A-train constellation, providing observations at 1:30 a.m./p.m. (descending/ascending) local time from June 2002 to October 2011. Here we use the NASA GES DISC Level 3 gridded, half-daily product V002 for AMSR-E-C and AMSR-E-X SM, expressed on the same regular  $1/4^\circ \times 1/4^\circ$  spatial grid as the AMSR2 products. The data is therefore similarly up-scaled to the same  $1/2^\circ \times 1/2^\circ$  working grid.

## 2.2. MERRA-L soil moisture

The MERRA is a re-analysis that combines in situ and remotely sensed observations of atmospheric conditions, radiance data from sounders, and wind retrievals from scatterometers (Rienecker et al., 2011). The MERRA-L, motivated by limitations in MERRA land surface hydrological fields, is a land-only analysis with meteorological forcing from MERRA model and more realistic precipitation forcing (Reichle et al., 2011). The surface SM estimates from MERRA-L are associated with the topmost (0–2 cm) soil layer. The MERRA-LSM are independent from those of AMSR-E and AMSR2 as the analysis does not use their brightness temperature observations during data assimilation. Accordingly, the MERRA-L SM data are used here for three purposes. First, they are used to distinguish two time periods from the AMSR-E era and the operating period of AMSR2, respectively, during which modeled SM conditions are statistically equivalent (see Section 3.1). Second, comparisons between satellite and model SM are made following Al-Yaari et al. (2014) and Parinussa et al. (2015); here MERRA-L SM is considered as reference data that reflect the spatial and temporal characteristic of SM. The MERRA-L SM is also known to correspond favorably to in-situ measurements across the world, including Australia (Albergel et al., 2013b). Finally, MERRA-L data serves as the instrument variable for estimating random errors in the AMSR-E and AMSR2 products in the LV analysis. MERRA-L has been used in a similar way in triple collocation analysis carried out by Draper et al. (2013) and Su et al. (2014a, 2014b).

## 3. Study area and methodology

### 3.1. Temporal sampling for four climate zones in Australia

The unavailability of common periods of data between AMSR-E and AMSR2 prevents a direct comparison of their error characteristics. To overcome this, one-year analysis time windows (January 1 to December 31) showing similar MERRA-L SM characteristics were selected for AMSR-E and AMSR2, respectively. First, the entire study region was divided into four climatic zones based on an aggregation of the Köppen-Geiger climate classification (Fig. 1) from Peel et al. (2007). Secondly, annual cumulative distribution functions (CDFs) of the daily MERRA-L time series of spatially averaged SM were used to represent each year's zonal SM characteristics. For each zone, we compared the CDFs from all of the possible pairs of yearly time windows (9 unimpaired years from 2003 to 2011 for AMSR-E  $\times$  2 unimpaired years from 2013 to 2014 for AMSR2 = 18 pairs), assessing their statistical similarity based on their root-mean-square difference (RMSD) and the Kolmogorov-Smirnov (K-S) test (Appendix A). The RMSD values were calculated as the difference between two CDFs, which were binned by percentiles increasing with 2% intervals (0–100%). In addition, the Kolmogorov-Smirnov (K-S) statistic was considered to quantify the similarity between two CDFs. These statistics identify our sampling periods for AMSR-E and AMSR2 between which fair comparisons are somewhat possible at the zonal level. The criteria for selection are that: i) the RMSD threshold is

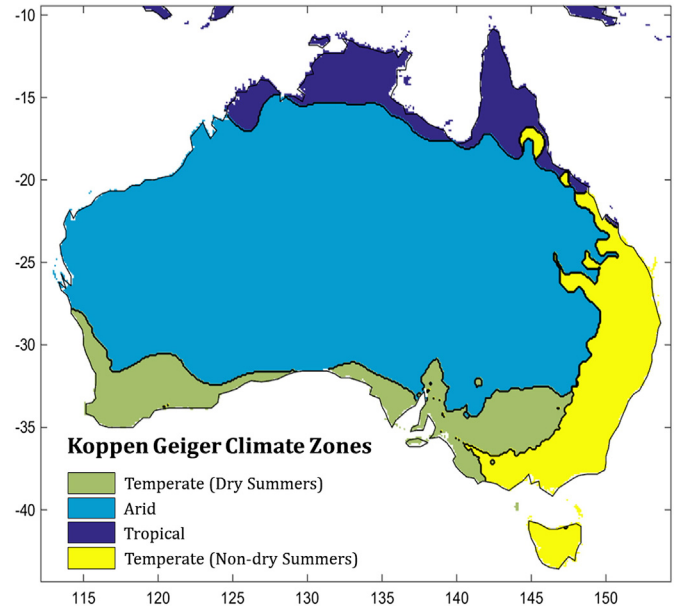


**Fig. 1.** Aggregated Koppen-Geiger climate map of Australia.

determined up to 0.01, and ii) the K-S test does not reject the null hypothesis ( $H_0$ ) that the two samples come from a population with the same distribution at 0.05 confidence level. For each zone, the pair of time windows with the smallest RMSD scores was chosen for further error characterization (and since for three of the four climate zones, and the associated K-S tests do not reject the null hypothesis).

Table 1 shows the RMSDs and K-S values for the 18 cases and the four climate zones. Three of the climate regions (Te-D, Ard, and Trp) have a case that meets the aforementioned criteria. For the Te-D region, model SM data during 2003 and 2014 (case 10) show statistical similarity, while for the Ard and Trp regions, the similarity exists between 2004 and 2014 model SM data (case 11). For the Te-ND region, case 5 (2007 c.f. 2013) was chosen based on the smallest RMSD value (0.009), even though the K-S test rejects the null hypothesis.

### 3.2. Lagged variable (LV) error estimator and comparison metrics

Two approaches were adopted to evaluate the satellite SM products. First, we quantify the differences between satellite and reference MERRA-L data using the Pearson's linear correlation coefficient  $R$ , and the unbiased root mean square difference (ubRMSD) where additive bias has been removed:

$$R = \frac{\text{cov}(S, M)}{\text{std}(S)\text{std}(M)} \quad (1)$$

$$\text{ubRMSD} = \sqrt{E\{(S - E(S)) - (M - E(M))\}^2} \quad (2)$$

where  $S$  refers to one of the satellite SM anomalies, and  $M$  represents the MERRA-L SM anomalies as the reference data.  $E(\cdot)$  computes the expectation value, and  $\text{cov}(\cdot)$  and  $\text{std}(\cdot)$  yield covariance and standard deviation statistics. ubRMSD has been used in previous studies of satellite SM (Albergel et al., 2013a; Dorigo et al., 2015; Kim et al., 2015). The correlation and ubRMSD can be degraded as a result of random errors in the modeled data, and ubRMSD can be also increased due to multiplicative bias between satellite and modeled SM (Su et al., 2015). Thus, these metrics are unable to characterize the intrinsic errors in the satellite products.

Accordingly, the second approach was undertaken to estimate their noise-to-signal ratio (NSR) of the satellite data using LV. The LV analysis

**Table 1**

Statistics of RMSD and K-S test between two CDFs of MERRA-L surface SM according to 4 climate zones (**Bold**: RMSD values below 0.01).

Case	Two MERRA's CDFs	Temperate (dry summers)			Arid			Tropical			Temperate (non-dry summers)		
		RMSD	K-S test	P-value	RMSD	K-S test	P-value	RMSD	K-S test	P-value	RMSD	K-S test	P-value
1	2003 vs 2013	<b>0.007</b>	reject	0.02	<b>0.006</b>	reject	0.00	0.025	reject	0.00	0.011	reject	0.00
2	2004 vs 2013	0.015	reject	0.00	<b>0.009</b>	reject	0.00	0.021	reject	0.00	0.020	reject	0.00
3	2005 vs 2013	0.011	reject	0.00	0.012	reject	0.00	0.019	reject	0.00	0.016	reject	0.00
4	2006 vs 2013	0.027	reject	0.00	0.015	reject	0.00	0.029	reject	0.00	0.031	reject	0.00
5	2007 vs 2013	0.016	reject	0.00	0.011	reject	0.00	0.023	reject	0.00	<b>0.009</b>	reject	0.00
6	2008 vs 2013	0.014	reject	0.00	<b>0.007</b>	reject	0.00	0.028	reject	0.00	0.012	reject	0.00
7	2009 vs 2013	<b>0.011</b>	reject	0.00	<b>0.007</b>	reject	0.00	0.027	reject	0.00	0.012	reject	0.00
8	2010 vs 2013	0.013	reject	0.00	0.042	reject	0.00	0.044	reject	0.00	0.031	reject	0.00
9	2011 vs 2013	0.031	reject	0.00	0.052	reject	0.00	0.043	reject	0.00	0.031	reject	0.00
10	2003 vs 2014	<b>0.005</b>	no reject	0.44	0.012	reject	0.00	0.019	reject	0.00	<b>0.010</b>	reject	0.00
11	2004 vs 2014	0.013	reject	0.00	<b>0.002</b>	no reject	0.56	<b>0.007</b>	no reject	0.17	0.018	reject	0.00
12	2005 vs 2014	<b>0.010</b>	reject	0.00	0.020	reject	0.00	0.019	reject	0.00	0.012	reject	0.00
13	2006 vs 2014	0.023	reject	0.00	<b>0.009</b>	reject	0.00	0.027	reject	0.00	0.026	reject	0.00
14	2007 vs 2014	<b>0.010</b>	reject	0.00	<b>0.005</b>	reject	0.00	0.021	reject	0.00	0.013	reject	0.00
15	2008 vs 2014	<b>0.010</b>	reject	0.00	<b>0.008</b>	reject	0.00	0.019	reject	0.00	0.017	reject	0.00
16	2009 vs 2014	<b>0.008</b>	reject	0.00	<b>0.005</b>	reject	0.00	0.013	reject	0.00	0.012	reject	0.00
17	2010 vs 2014	<b>0.010</b>	reject	0.00	0.035	reject	0.00	0.048	reject	0.00	0.040	reject	0.00
18	2011 vs 2014	0.026	reject	0.00	0.042	reject	0.00	0.038	reject	0.00	0.040	reject	0.00

no reject ( $H = 0$ ). Do not reject the null hypothesis at significance level (0.05).

reject ( $H = 1$ ). Reject the null hypothesis at significance level (0.05).

is based on strong autocorrelation characteristics of the geophysical variable of interest (SM). In particular, the standard deviation (std) of random error ( $\varepsilon_S$ ) existing in the individual satellite SM product ( $S$ ),  $\text{std}(\varepsilon_S)$ , is estimated, using MERRA-LSM as the lagged instrument. The MERRA-L as the lagged instrument takes advantage of its high temporal resolution and the availability of the model data, allowing error estimation over short time window (one year in this case). The errors in nighttime SM data were estimated, using variable lags  $m$  of MERRA-L:

$$\text{std}^2(\varepsilon_S) = \text{var}(S) - \frac{\text{cov}(S_t, M_t)\text{cov}(S_{t+m}, M_{t+m})}{\text{cov}(M_t, M_{t+m})} \quad (3)$$

where the subscripts  $t$  and  $t + m$  are used to distinguish lag covariance and  $m = 1$  indicates one-day lag, following Su et al. (2014a). The random error std metric does not necessarily represent the best measure of merits because it is influenced by the arbitrary scaling of  $S$ . The noise-to-signal ratio (NSR) thus serves as an alternative error metric:

$$\text{NSR}_S = \frac{\text{std}(\varepsilon_S)}{\text{std}(S)} \quad (4)$$

The SM data can have seasonal variations, so it is generally recommended that LV analysis be applied to SM anomalies (Miralles et al., 2010). In this study, the anomalies were defined as deviations from a 31-day moving average (Albergel et al., 2012; Su et al., 2014a, 2014b).

#### 4. Results and discussion

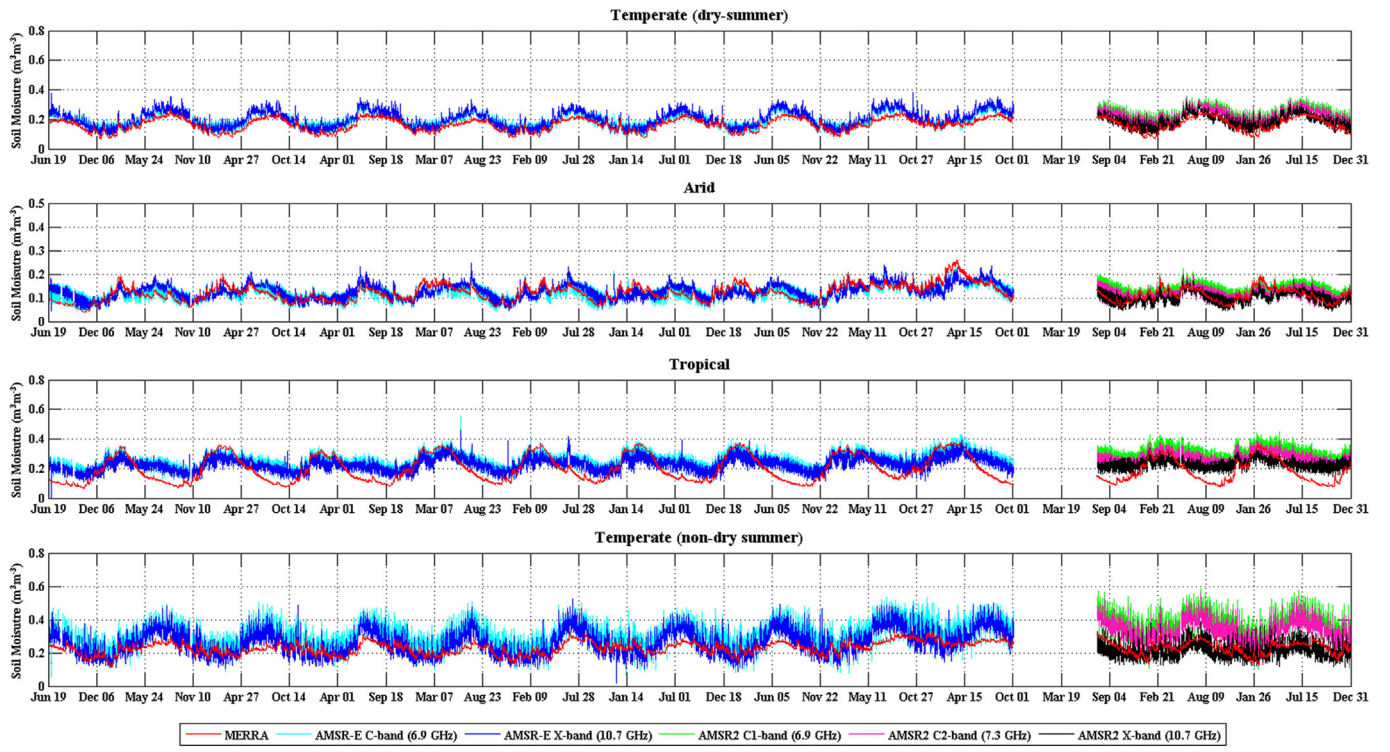
##### 4.1. Comparisons between AMSR2 and AMSR-E C-/X-band products with MERRA-L SM products

Fig. 2 shows the time series of AMSR-E-C and -X SM from July 2002 to October 2011 and AMSR2-C1, -C2, and -X SM from July 2012 to September 2014 with MERRA-L surface SM. The time series for each product represent zonal daily average values for each climate zone (Te-D, Ard, Trp, and Te-ND). All AMSR2 SM products exhibit similar temporal patterns to those of AMSR-E SM for each climate zone. Both AMSR-E-X and AMSR2-X SM show lower biases relative to MERRA-L SM, compared to AMSR-E/2-C SM, especially in the Trp and Te-ND climate zones. Figs. 3–6 evaluate inter-comparisons between AMSR-E and AMSR2 data against MERRA-L. It should be emphasized that pixel-to-pixel spatial comparisons between AMSR-E and AMSR2 in Figs. 3–5 must be

interpreted with caution, because SM dynamics and land-surface characteristics between the two selected years can differ at the pixel level. Generally speaking, the zonal time series of AMSR-E SM and AMSR2 SM (C- and X-bands) show similar temporal variations to the MERRA-L SM data during their respective periods, although visible biases are present almost evenly among AMSR-E and AMSR2 in the Trp and Te-ND regions (Fig. 2). These analyses also show that the C-band SM products have slightly higher biases than the X-band SM. Figs. 3 and 4 show spatial comparisons of ubRMSD and the correlation between AMSR-E/2 C- and X-band SM and MERRA-L SM anomalies over Australia. The pairs of AMSR-E and AMSR2 maps show very similar spatial patterns, which is confirmed by the boxplots of metrics (see also Fig. 6) with higher ubRMSD over the eastern seaboards (Fig. 3) and higher  $R$  observed over the temperate (Te-D and Te-ND) and semi-arid regions (Fig. 4). The notable difference between AMSR-E and AMSR2 is that AMSR2-X shows lower ubRMSD in temperate (Te-ND) southeastern regions, and AMSR-E C- and X-bands have notably lower ubRMSD in parts of the arid zone.

The comparisons of other configurations are summarized in Fig. 5. This figure compares the metrics, ubRMSD and  $R$ , at the pixel level for the C- and X-band SM products across the four climate zones. Despite SM variability at the pixel level between the sampled years, there is agreement between two satellite-based ubRMSD metrics, especially for the Ard and Trp zones. Partitioning the number of pixels with a 1:1 line, we found that the ubRMSD of AMSR2-C was higher than that of AMSR-E-C for all climate zones, with pixel percentages being 78.0, 73.4, 71.0, and 80.1% for Te-D, Ard, Trp, and, Te-ND, respectively (Fig. 5a). The percentages of pixels where AMSR2-X are higher than those of AMSR-E-X are 66.6, 71.7, and 52.0% for Te-D, Ard, and Trp, excluding the opposing case of Te-ND with 39.2% (Fig. 5b). Fig. 5c and d show that, for  $R$ -values, AMSR-E-C and -X are slightly superior to AMSR2, with the exception of the Trp zone; the C-band yields relative percentages of 55.0, 52.1, and 61.5%, and the X-band percentages of 55.1, 50.9, and 54.0% for Te-D, Ard, and Te-ND, respectively.

Fig. 6 shows the zonal statistics of the metrics, which are arguably more representative of the relative merits of the satellite SM products, based on our chosen zonal sampling strategy. The statistics of ubRMSD and  $R$ , namely their first quartile, median and third quartile, are summarized with boxplots. A comparison between AMSR-E-C and X products reveals that the X-band has a slightly higher ubRMSD in the Trp and Te-ND zones, with median statistics of 0.042 and  $0.050 \text{ m}^3 \text{ m}^{-3}$  and 0.039 and  $0.046 \text{ m}^3 \text{ m}^{-3}$  due to multiplicative bias. This could be partly



**Fig. 2.** Time series of AMSR-E (C/X-band) soil moisture from July 2002 to October 2011 and AMSR2 (C1/C2/X-band) soil moisture from July 2012 to September 2014 and MERRA-L surface moisture for the whole period.

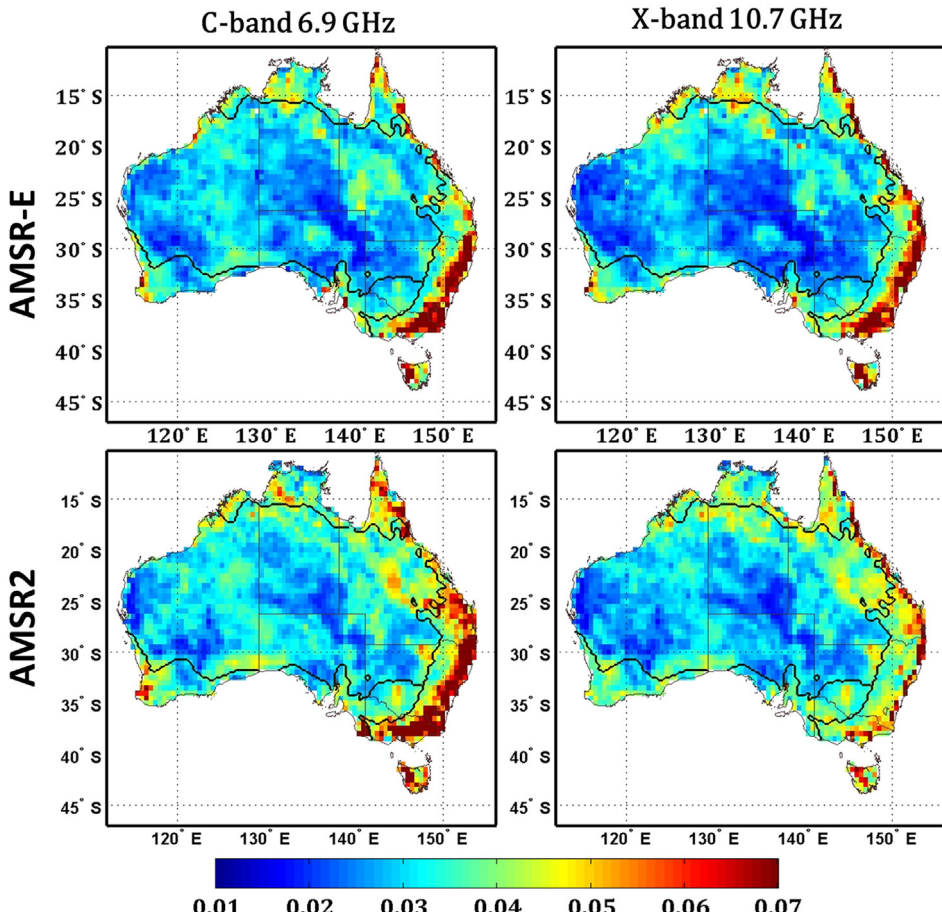


**Fig. 3.** Spatial maps of unbiased RMSD of AMSR-E/2 C-band (6.9 GHz) and X-band (10.7 GHz) SM anomalies compared to MERRA-L SM anomaly over Australia.

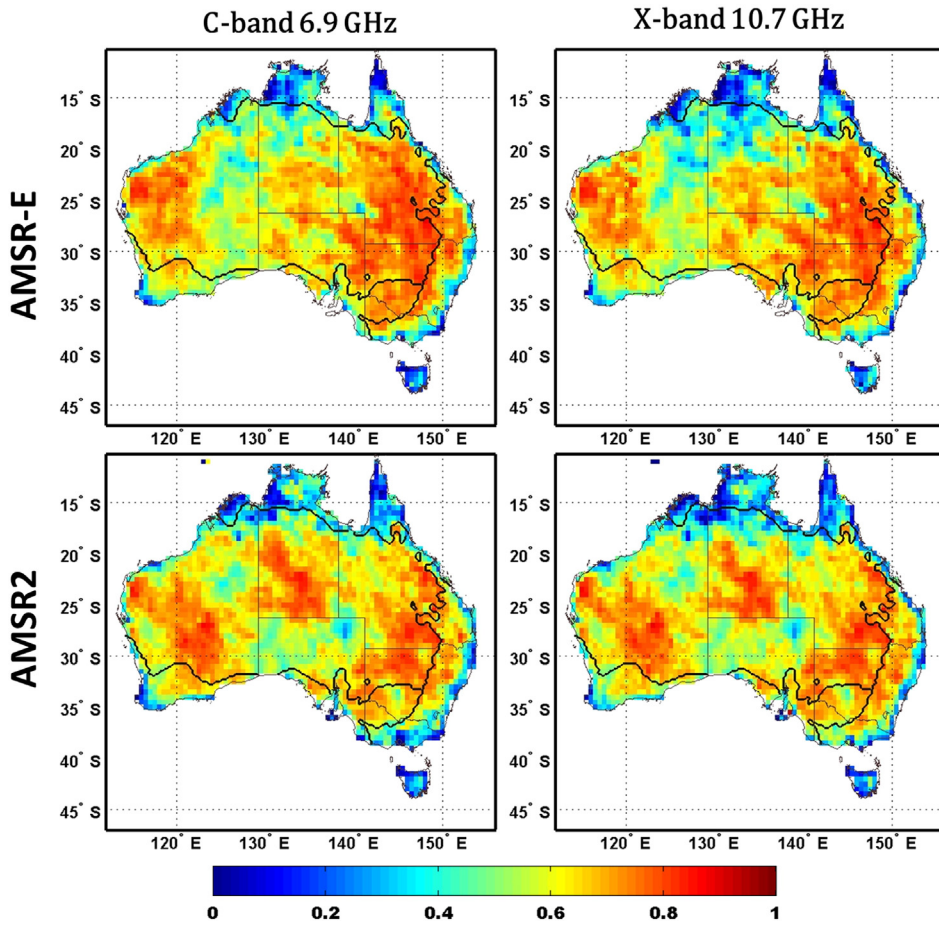


**Fig. 4.** Spatial maps of R-value between AMSR-E/2 C-band (6.9 GHz) and X-band (10.7 GHz) SM anomalies and MERRA-L SM anomaly over Australia.

attributed to differences in representative depths between the model and satellite SM. Additionally,  $R$  of X-band is marginally lower than C-band in the Trp zone (0.27 c.f. 0.32) as a result of larger random errors. C-band has a longer sensing depth and thus is expected to be less susceptible to vegetation masking compared to X-band (Cho et al., 2015b; Draper et al., 2009). However, this contrasts between C- and X-band data is not consistent with AMSR2. Moreover, AMSR2 C-band shows higher ubRMSD than AMSR-E C-band, especially in the Trp and Te-ND zones. One possible reason is the difficulty to conduct intercalibration procedure for the AMSR2's C-band observations. Currently, the intercalibration between X-band observations from AMSR-E and AMSR2 can rely on overlapping X-band observations from the TRMM satellite (Parinussa et al., 2015), but this approach is not immediately applicable to the C-band. Consequently, the differences in ubRMSD between AMSR2 and AMSR-E C-bands are relatively large, with a maximum of  $0.09 \text{ m}^3 \text{ m}^{-3}$ , and differences in  $R$  of up to 0.07, compared to the X-bands.

As a whole, the zonal dependency of ubRMSD and  $R$  values are similar between the AMSR2 and AMSR-E products. In particular, their ubRMSD values are generally lower in Te-D and Ard zones, while  $R$  values are also highest in the Te-D and Ard zones. Further, in a comparison with MERRA-L data, AMSR-E and AMSR2-X are generally very similar. The correlation-based accuracy of ascending SM retrievals is presented in Appendix C.

#### 4.2. Comparisons of AMSR2 and AMSR-E error estimates

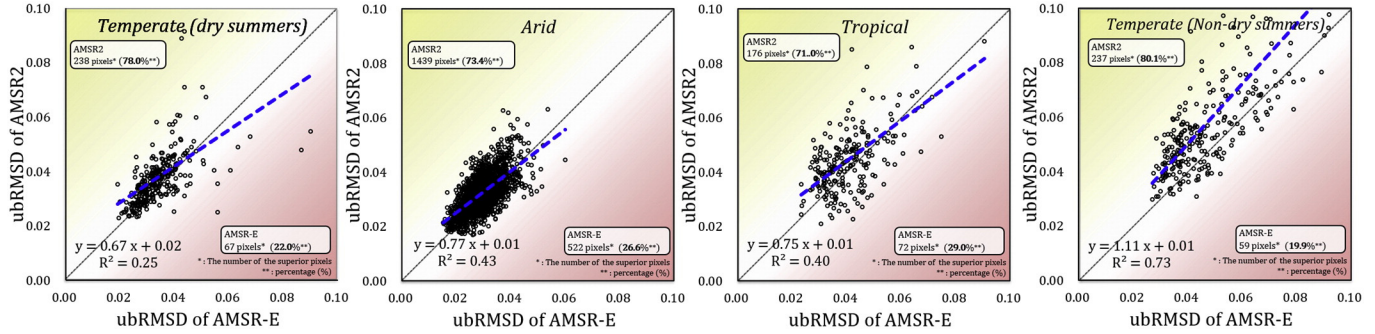
Figs. 7–8 depict the spatial maps of random error std for AMSR-E and AMSR2, and Fig. 9 provides their zonal statistics. Comparing the C- and X-bands, the error std estimates are generally similar across the

continent for both AMSR-E and AMSR2. Exceptions can be seen in parts of eastern seaboard in Te-ND for AMSR2, which is confirmed by the boxplots (Fig. 9b and d). Additionally, between AMSR-E-C and AMSR2-C, the latter shows higher error std for all zones, with the zonal median error std being slightly higher by  $0.01 \text{ m}^3 \text{ m}^{-3}$  at most, whereas in the X-band, the latter shows lower error std for Trp and Te-ND zones. In fact, the error std maps display general correspondence with the climate characteristics (Fig. 1), and there are spatial similarities among the products. The zonal differences of error std support the expectation that the spatial variability of error std mirrors the overall soil wetness conditions because retrieval SM and retrieval error is jointly scaled by the field capacity of soil. The Te-ND zone is associated with higher error std across all the products, with the lowest error in the Ard zone.

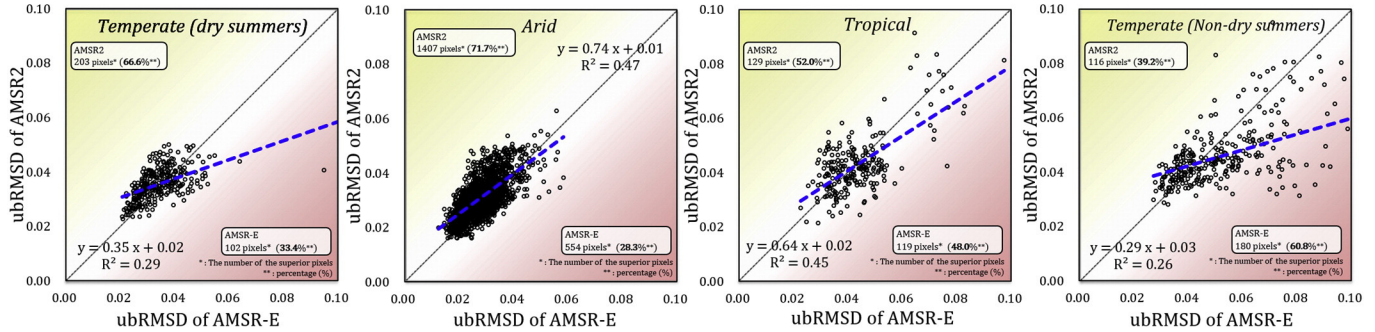
Furthermore, there is also a visible association of error std with land surface characteristics. Eastern and southwestern regions are dominated by higher tree cover and urban land uses, compared to the arid and semi-arid central region that makes up 70% of Australia, which is dominated by deserts, shrubs, and grasses. The corresponding spatial patterns of error std are expected, since that the quality of passive SM retrievals at a coarse scale diminishes with vegetation density and spatial heterogeneity (Loew, 2008; Brocca et al., 2011). For these regions, it appears to be consistent with the previous error evaluation carried out by Su et al. (2014b), although they analyzed the errors in descending and ascending SM retrievals jointly.

Fig. 8 and Fig. 9e-h show complementary results based on NSR as a scaling-independent metric. The NSR metric partially mirrors the correlation results in Fig. 4(d-f), as a higher NSR in the satellite data leads to diminished correlation with the MERRA-L data. However, larger error std does not necessarily lead to higher NSR. For instance, the Te-ND

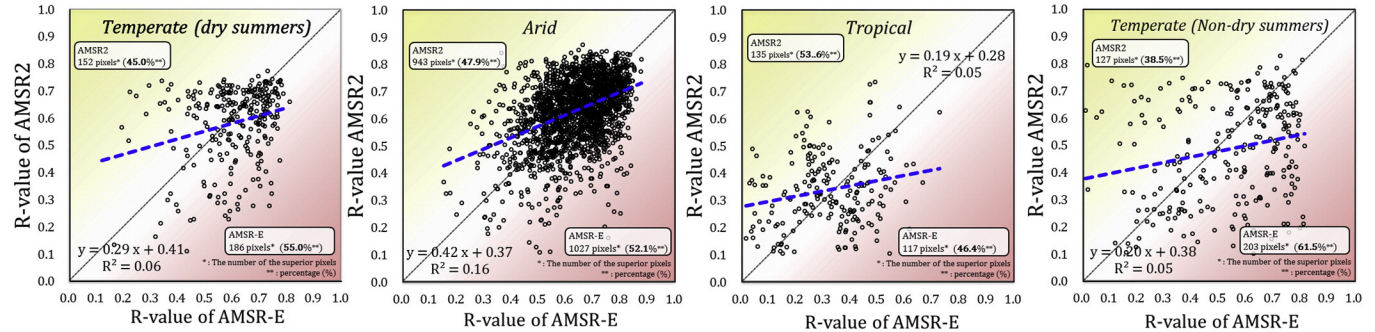
a) ubRMSD of C-band between AMSR-E and AMSR2



b) ubRMSD of X-band between AMSR-E and AMSR2



c) R-value of C-band between AMSR-E and AMSR2



d) R-value of X-band between AMSR-E and AMSR2

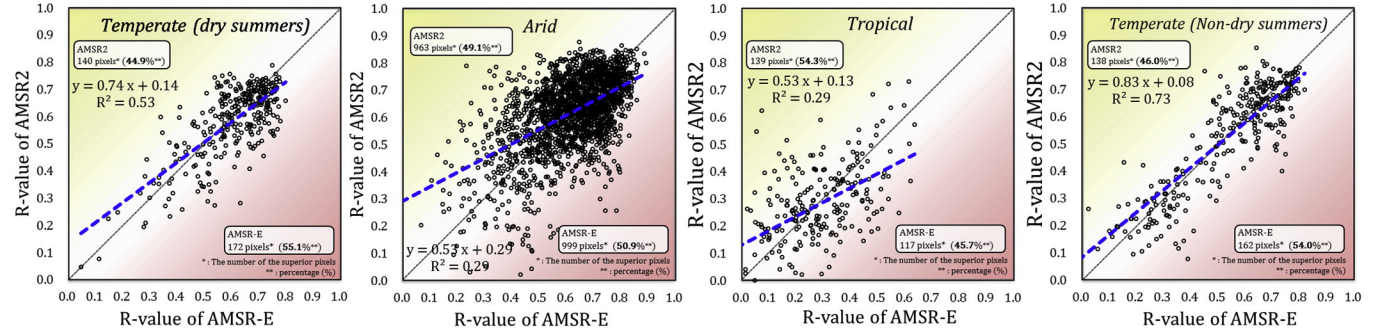


**Fig. 5.** Comparisons of unbiased RMSD (a, b) and R-value (c, d) between AMSR-E and AMSR2 C- and X-band SM anomalies from calculating with MERRA-L SM anomaly for four climate zones.

zone has the second highest median NSR (0.72–0.78), but has the highest median error std (Fig. 9). The low zonal median error std in Arid is associated with the lowest median NSR (0.65–0.70) and a relatively higher median *R* (0.64–0.65) due to low SM variability at low moisture levels in this region. In the Trp region, the high median NSR (0.90–0.92) and lower median *R* (0.27–0.33) may be related to the low quality of microwave signals as well as the high SM variability

over the dense vegetation cover (Al-Yaari et al., 2014; Chakravorty et al., 2016). It also could be due to relatively low quality of MERRA-L SM over forested areas, compared to non-forested areas (Yi et al., 2011). SM retrievals over Te-D and Te-ND regions show relatively higher median NSR, ranging from 0.72 to 0.75 and 0.72 to 0.78, respectively. There are notable spatial similarities in NSR across the satellite products. Given the spatiotemporal coincidence of the data and analysis period,

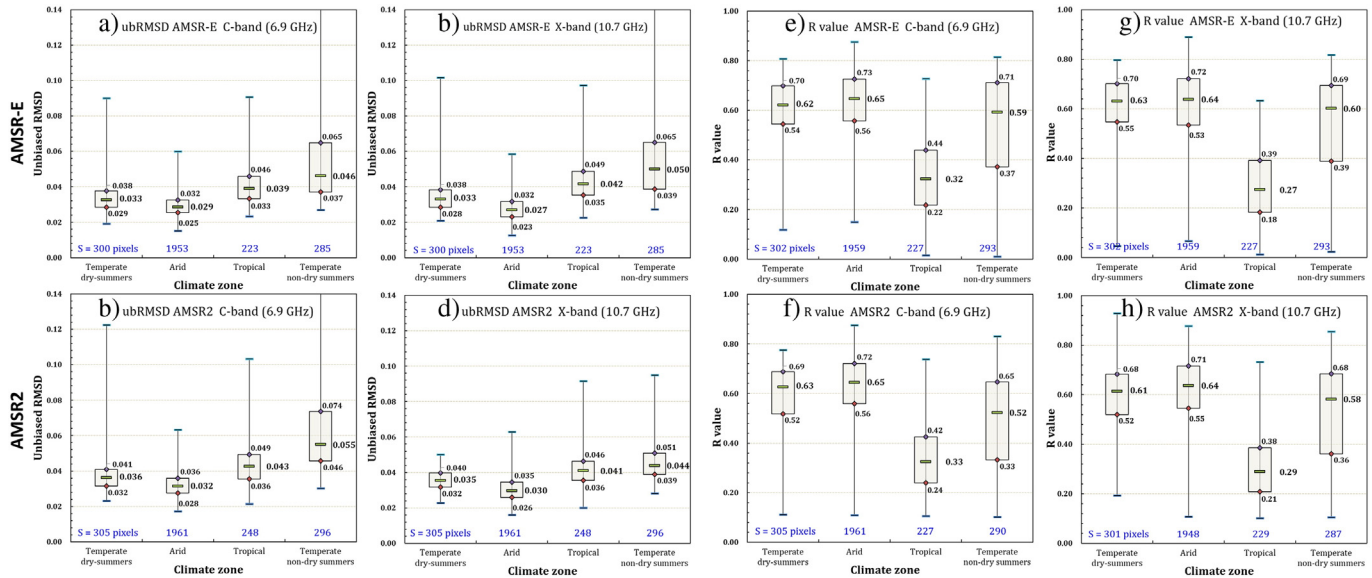


Fig. 6. Four climate zonal statistics of the unbiased RMSD and R-value for (a, e) AMSR-E C-band, (c, g) AMSR-E X-band, (b, f) AMSR2 C-band, and (d, h) AMSR2 X-band SM anomalies.

the NSR maps of AMSR-E/2 C and X-band SM are similar across the continent. However, the NSR maps of AMSR2-X are visibly different from AMSR-E in parts of the Ard and Trp zones in Fig. 8. This could be attributed to differences in the meteorological and land surface characteristics between the two analysis periods for AMSR2 and AMSR-E, even though the modeled SM conditions, which may be erroneous, are similar on the

basis of our tests. Our results therefore suggest that this may lead to spatial differences in random errors. Furthermore, pixel-level statistics may not accurately map monotonically to zonal summary statistics. Future work should consider data sampling strategies implemented at the pixel level and the use of other ancillary data on, for example, vegetation, rainfall, and land surface temperature, to enhance diagnosis.

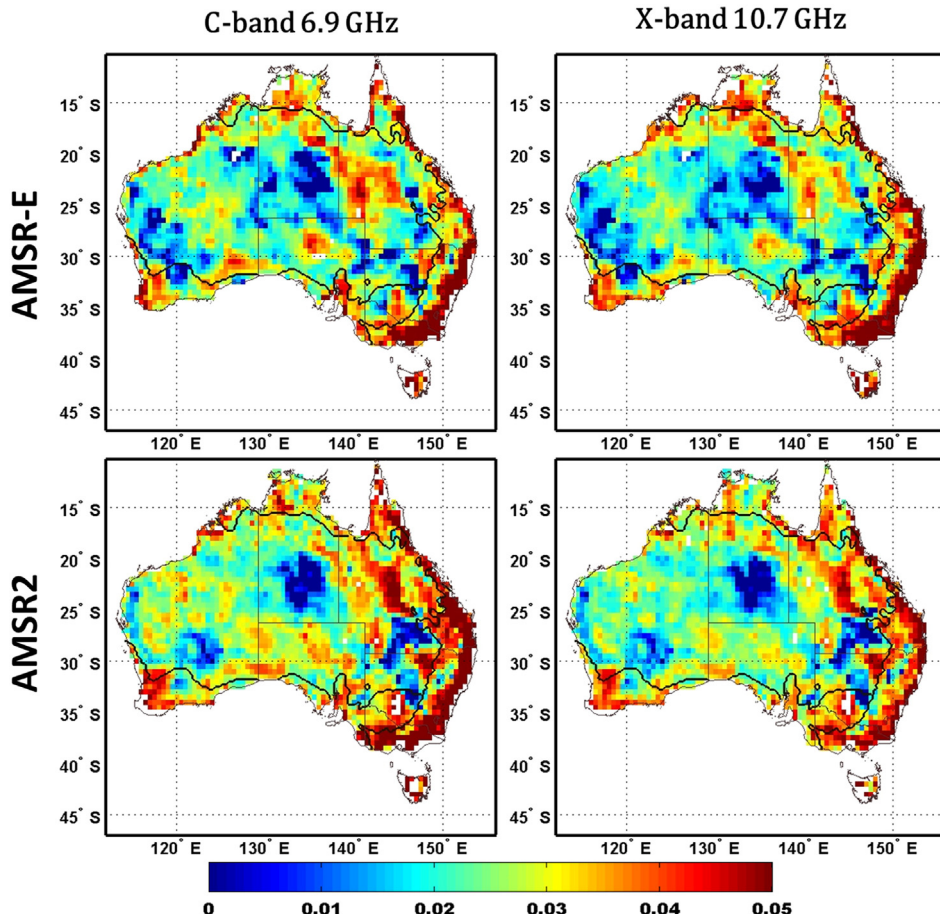
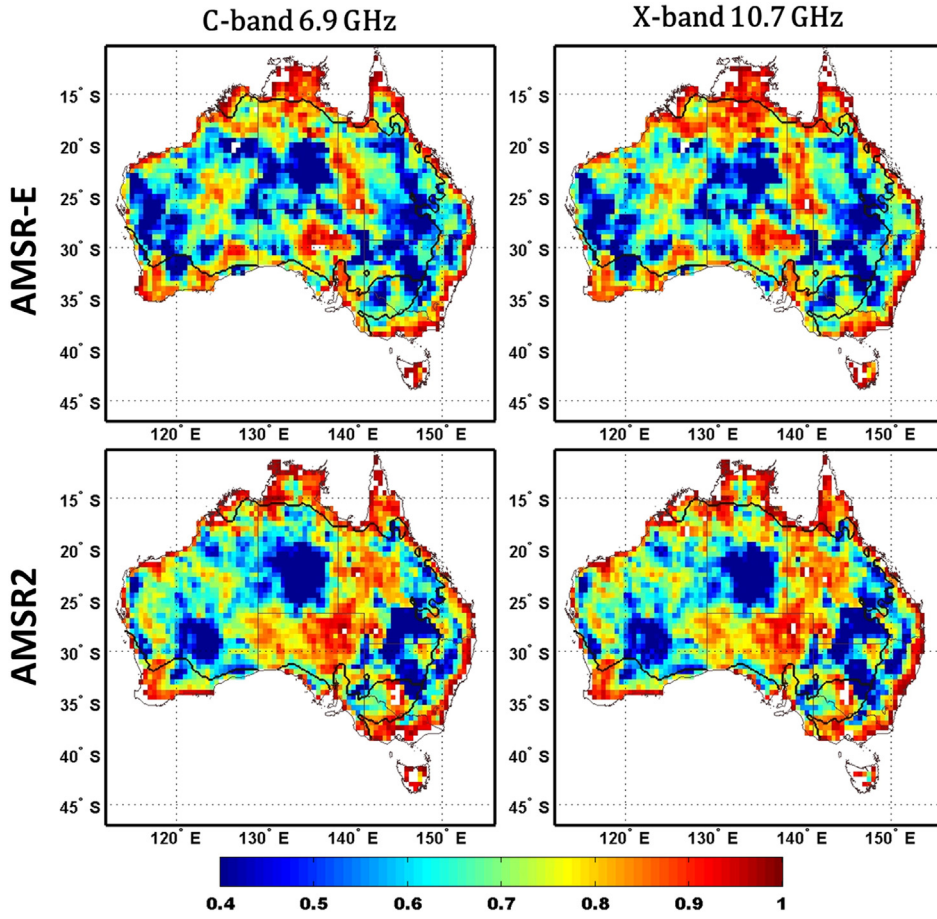


Fig. 7. Spatial maps of error standard deviation of AMSR-E/2 C-band (6.9 GHz) and X-band (10.7 GHz) SM anomalies over Australia, estimated using LV error estimator.



**Fig. 8.** Same as Fig. 7, but NSR estimates are plotted and compared.

Based on the bulk statistics, and with minimal RFI in the regions, the results show no superiority of AMSR2 LPRM C- and X-bands retrievals over AMSR-E in terms of error std and NSR. This may be related to the calibration difference between AMSR2 and AMSR-E (Okuyama and Imaoka,

2015). The calibration process can lead to changes of scaling of the SM data (De Lannoy et al., 2013), which can influence the multiplicative bias. The lack of additional calibration processes for AMSR2 data could offset the effect of instrumental improvements in AMSR2 on SM retrievals.

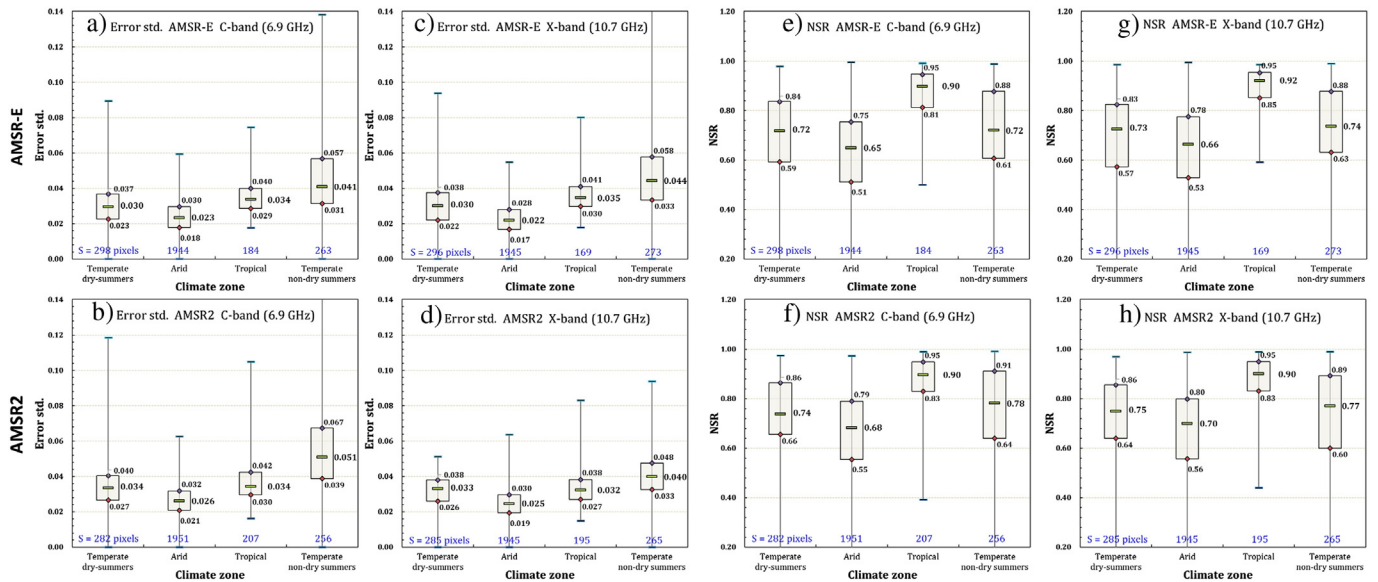


**Fig. 9.** Four climate zonal statistics of error standard deviations and NSR for (a, d) AMSR-E C-band (6.9 GHz), (b, e) AMSR-E X-band (10.7 GHz), and (c, f) AMSR2 X-band (10.7 GHz) SM anomalies.

## 5. Conclusions

This work presents an inter-comparison of AMSR2 and AMSR-E SM (C- and X-band) retrievals over Australia. We ensured retrieval algorithmic consistency between two sensors by using the LPRM products and minimal intra-annual differences in SM conditions between analysis periods for the two sensors. The latter was achieved through the use of CDFs of the MERRA-L SM time series to select comparable one-year time periods in which SM conditions are statistically equivalent on a zonal scale. It was found that AMSR-E and AMSR2 C- and X-band products showed comparable agreement with MERRA-L SM. For the ubRMSD values, AMSR-E C-band SM had better agreements than AMSR2 C-band with median ubRMSD (AMSR-E: 0.029 to 0.046 m<sup>3</sup> m<sup>-3</sup>, AMSR2: 0.032 to 0.055 m<sup>3</sup> m<sup>-3</sup>). Also, AMSR-E X-band showed slightly better agreements compared to AMSR2 across three climate zones (AMSR-E: 0.027 to 0.042 m<sup>3</sup> m<sup>-3</sup>, AMSR2: 0.030 to 0.041 m<sup>3</sup> m<sup>-3</sup>), with the exception of relatively high ubRMSD of 0.050 m<sup>3</sup> m<sup>-3</sup> (AMSR2: 0.044 m<sup>3</sup> m<sup>-3</sup>) in the Te-ND zone. The correlation (*R*-value) of AMSR2 C- & X-band SM was generally similar with those of AMSR-E, with a maximum difference in *R* of 0.07 in the Te-ND zone. When the same metrics were used to compare X-band against C-band, AMSR-E and AMSR2 X-band SM showed similar zonal distributions to the C-band SM, but differences were perceptible in the Ard zones (AMSR-E/2 C-band: 0.32/0.33, AMSR-E/2 X-band: 0.27/0.29). With the additional metrics, error std, and NSR being used, the results revealed that the error maps of AMSR2 & AMSR-E C and X-band were zonally similar over the four Australian regions. However, the noticeable differences in error std and NSR between AMSR-E and AMSR2 were confirmed when their boxplots were used. For both frequencies, the error of AMSR2 were higher than AMSR-E in the two drier zones (Te-D and Arid) and there was no clear superiority of AMSR2 in the two wetter zones (Te-ND and Trp).

This study concludes that there is little evidence to support the benefits of the improved instrumental design of AMSR2 in improving SM retrievals, compared to AMSR-E. There could be several possible reasons. First, the differences may be too small to be recognized at a coarse-scale (50 km) resolution and in zonal statistics. Second, when MERRA-L is used as reference, the model error could be larger than the differences in accuracy, such that the latter cannot be resolved. Lastly, the LPRM algorithm, which essentially relates calibrated brightness temperature data to soil moisture values, may not be able to propagate the influence of instrumental improvements in order to achieve enhanced retrievals. The differences between NASA's LPRM AMSR2 C-band products and the X-band product, and those between the two versions of AMSR2 C-band products reflect the adverse impacts of incorrect calibration of AMSR2 brightness temperatures on its SM retrievals. They have shown to lead to significant systematic biases, resulting in changes to the short time-scale and seasonal dynamics of retrieved SM. These data illustrate the importance of using properly calibrated brightness temperature data prior to retrievals. With ongoing efforts to improve the calibration of AMSR2 data, improvements to retrieved SM can be expected, yet at this point, the similarities between AMSR-E and AMSR2 SM suggest that AMSR2 & AMSR-E combination provides a valuable asset for continuous passive microwave SM retrievals. Future work may consider the use of land surface information to revise the sampling strategy and to investigate the pixel-level differences between AMSR2 and AMSR-E.

Supplementary data to this article can be found online at <http://dx.doi.org/10.1016/j.rse.2016.10.050>.

## Acknowledgements

The authors are grateful to all who contributed to the data sets used in this study. We would also like to thank the editor and three anonymous reviewers for their valuable comments on the manuscript. The AMSR2 and AMSR-E LPRM data were produced by Richard de Jeu

(VUA), Robert Parinussa (UNSW), and colleagues at NASA. The AMSR2 LPRM V001, AMSR-E LPRM V002, and MERRA-L SM datasets were downloaded from the NASA Goddard Earth Sciences Data and Information Services Center (GES-DISC). The most recent AMSR2 LPRM SM datasets were personally provided by Dr. Parinussa. This research was supported by the Space Core Technology Development Program through the National Research Foundation of Korea (NRF) funded by the Ministry of Science, ICT and Future Planning (NRF-2014M1A3A3A02034789).

## References

- Alvarez-Garreton, C., Ryu, D., Western, A.W., Su, C.-H., Crow, W.T., Robertson, D.E., Leahy, C., 2015. Improving operational flood ensemble prediction by the assimilation of satellite soil moisture: comparison between lumped and semi-distributed schemes. *Hydrol. Earth Syst. Sci.* 19, 1659–1676.
- Albergel, C., Brocca, L., Wagner, W., de Rosnay, P., Calvet, J.-C., 2013a. Selection of performance metrics for global soil moisture products: the case of ASCAT product. *Remote Sensing of Energy Fluxes and Soil Moisture Content*. CRC Press:pp. 427–444 <http://dx.doi.org/10.1201/b15610-22> Chapter: 18.
- Albergel, C., de Rosnay, P., Gruhier, C., Muñoz Sabater, J., Hasenauer, S., Isaksen, L., et al., 2012. Evaluation of remotely sensed and modeled soil moisture products using global ground-based in situ observations. *Remote Sens. Environ.* 118, 215–226.
- Albergel, C., Dorigo, W., Reichle, R., Balsamo, G., Rosnay, P.d., Muñoz-Sabater, J., et al., 2013b. Skill and global trend analysis of soil moisture from reanalyses and microwave remote sensing. *J. Hydrometeorol.* 14, 1259–1277.
- Al-Yaari, A., Wigneron, J.-P., Ducharme, A., Kerr, Y., de Rosnay, P., de Jeu, R., et al., 2014. Global-scale evaluation of two satellite-based passive microwave soil moisture datasets (SMOS and AMSR-E) with respect to land data assimilation system estimates. *Remote Sens. Environ.* 147, 181–195.
- Bolten, J.D., Crow, W.T., Zhan, X., Reynolds, C., Jackson, T.J., 2009. Assimilation of a satellite-based soil moisture product in a two-layer water balance model for a global crop production decision support system. *Data Assimilation for Atmospheric, Oceanic, and Hydrologic Applications*. Springer, Berlin:pp. 449–463 [http://dx.doi.org/10.1007/978-3-540-71056-1\\_23](http://dx.doi.org/10.1007/978-3-540-71056-1_23).
- Bolten, J.D., Crow, W.T., Zhan, X., Jackson, T.J., Reynolds, C.A., 2010. Evaluating the utility of remotely sensed soil moisture retrievals for operational agricultural drought monitoring. *IEEE J. Sel. Top. Appl. Earth Obs. Remote Sens.* 3 (1):57–66. <http://dx.doi.org/10.1109/JSTARS.2009.2037163>.
- Brocca, L., Melone, F., Moramarco, T., Wagner, W., Naeimi, V., Bartalis, Z., et al., 2010. Improving runoff prediction through the assimilation of the ASCAT soil moisture product. *Hydrol. Earth Syst. Sci.* 14 (10), 1881–1893.
- Brocca, L., Hasenauer, S., Lacava, T., Melone, F., Moramarco, T., Wagner, W., et al., 2011. Soil moisture estimation through ASCAT and AMSR-E sensors: An intercomparison and validation study across Europe. *Remote Sens. Environ.* 115, 3390–3408.
- Chakravorty, A., Chahar, B.R., Sharma, O.P., Dhanya, C.T., 2016. A regional scale performance evaluation of SMOS and ESA-CCI soil moisture products over India with simulated soil moisture from MERRA-Land. *Remote Sens. Environ.* 186, 514–527.
- Champagne, C., Berg, A., Belanger, J., McNairn, H., De Jeu, R.A.M., 2010. Evaluation of soil moisture derived from passive microwave remote sensing over agricultural sites in Canada using ground-based soil moisture monitoring networks. *Int. J. Remote Sens.* 31, 3669–3690.
- Cho, E., Moon, H., Choi, M., 2015a. First assessment of the advanced microwave scanning radiometer 2 (AMSR2) soil moisture contents in northeast Asia. *J. Meteorol. Soc. Jpn.* 93 (1):139–151. <http://dx.doi.org/10.2151/jmsj.2015-008>.
- Cho, E., Choi, M., Wagner, W., 2015b. An assessment of remotely sensed surface and root zone soil moisture through active and passive sensors in northeast Asia. *Remote Sens. Environ.* 160:166–179. <http://dx.doi.org/10.1016/j.rse.2015.01.013>.
- Choi, M., Jacobs, J.M., Anderson, M.C., Bosh, D.D., 2013. Evaluation of drought indices via remotely sensed data with hydrological variables. *J. Hydrol.* 476, 265–273.
- Crow, W.T., Wood, E.F., 2002. The value of coarse-scale soil moisture observations for regional surface energy balance modeling. *J. Hydrometeorol.* 3, 467–482.
- Crow, W.T., van den Berg, M.J., Huffman, G.J., Pellarin, T., 2011. Correcting rainfall using satellite-based surface soil moisture retrievals: the soil moisture analysis rainfall tool (SMART). *Water Resour. Res.* 47, W08521. <http://dx.doi.org/10.1029/2011WR010576>.
- De Jeu, R.A.M., Dorigo, W.A., Parinussa, R.M., Wagner, W., Chung, D., 2012. [Global climate] building a climate record of soil moisture from historical satellite observations [in: state of the climate in 2011]. *Bull. Am. Meteorol. Soc.* 93, S32–S33.
- De Lannoy, G.J.M., Reichle, R.H., Pauwels, V.R.N., 2013. Global calibration of the GEOS-5 L-band microwave radiative transfer model over nonfrozen land using SMOS observations. *J. Hydrometeorol.* 14, 765–785.
- Dorigo, W.A., Gruber, A., De Jeu, R.A.M., Wagner, W., Stacke, T., Loew, A., Albergel, C., Brocca, L., Chung, D., Parinussa, R.M., Kidd, R., 2015. Evaluation of the ESA CCI soil moisture product using ground-based observations. *Remote Sens. Environ.* 162, 380–395.
- Draper, C.S., Walker, J.P., Steinle, P.J., de Jeu, R.A.M., Holmes, T.R.H., 2009. An evaluation of AMSR-E derived soil moisture over Australia. *Remote Sens. Environ.* 113, 703–710.
- Draper, C.S., Reichle, R.H., De Lannoy, G.J.M., Liu, Q., 2012. Assimilation of passive and active microwave soil moisture retrievals. *Geophys. Res. Lett.* 39:L04401. <http://dx.doi.org/10.1029/2011GL050655>.
- Draper, C.S., Reichle, R.H., de Jeu, R.A., Naeimi, V., Parinussa, R.M., Wagner, W., 2013. Estimating root mean square errors in remotely sensed soil moisture over continental scale domains. *Remote Sens. Environ.* 137, 288–298.

- Gruhier, C., De Rosnay, P., Hasenauer, S., Holmes, T., De Jeu, R., Kerr, Y., Mougin, E., Njoku, E., Timouk, F., Wagner, W., Zribi, M., 2010. Soil moisture active and passive microwave products: intercomparison and evaluation over a Sahelian site. *Hydrol. Earth Syst. Sci.* 14:141–156. <http://dx.doi.org/10.5194/hess-14-141-2010>.
- Imaoaka, K., Kachi, M., Kasahara, M., Ito, N., Nakagawa, K., Oki, T., 2010. Instrument performance and calibration of AMSR-E and AMSR2. *Int. Arch. Photogramm. Remote. Sens. Spat. Inf. Sci.* 13–16 XXXVIII, Part 8.
- Jackson, T.J., Cosh, M.H., Bindlish, R., Starks, P.J., Bosch, D.D., Seyfried, M., Goodrich, D.C., Moran, M.S., Du, J., 2010. Validation of advanced microwave scanning radiometer soil moisture products. *IEEE Trans. Geosci. Remote Sens.* 48 (12), 4256–4272.
- Jung, M., Reichstein, M., Ciais, P., Seneviratne, S.I., Sheffield, J., Goulden, M.L., et al., 2010. Recent decline in the global land evapotranspiration trend due to limited moisture supply. *Nature* 467, 951–954.
- Kim, S., Liu, Y.Y., Johnson, F.M., Parinussa, R.M., Sharma, A., 2015. A global comparison of alternate AMSR2 soil moisture products: why do they differ? *Remote Sens. Environ.* 161, 43–62.
- Koike, T., 2013. Description of the GCOM-W1 AMSR2 Soil Moisture Algorithm, Technical Report—Description of the GCOM-W1 Level 1R and Level 2 Algorithms. Japan Aerospace Exploration Agency (JAXA) Earth Observation Research Center, pp. 8.1–8.13 NDX-120015A, Chapter 8.
- Lei, F., Crow, W.T., Shen, H., Parinussa, R.M., Holmes, T.R.H., 2015. The impact of local acquisition time on the accuracy of microwave surface soil moisture retrievals over the contiguous United States. *Remote Sens.* 7 (10), 13448–13465.
- Loew, A., 2008. Impact of surface heterogeneity on surface soil moisture retrievals from passive microwave data at the regional scale: the upper Danube case. *Remote Sens. Environ.* 112 (1), 231–248.
- Miralles, D.G., van den Berg, M.J., Gash, J.P., Jeu, R., Beck, H.E., et al., 2014. El Niño–La Niña cycle and recent trends in continental evaporation. *Nat. Clim. Chang.* 4, 122–126.
- Miralles, D.G., Crow, W.T., Cosh, M.H., 2010. Estimating spatial sampling errors in coarse-scale soil moisture estimates derived from point-scale observations. *J. Hydrometeorol.* 11, 1423–1429.
- Mladenova, I.B., Jackson, T.J., Njoku, E., Bindlish, R., Chan, S., Cosh, M.H., et al., 2014. Remote monitoring of soil moisture using passive microwave-based techniques – theoretical basis and overview of selected algorithms for AMSR-E. *Remote Sens. Environ.* 144, 197–213.
- Njoku, E.G., Jackson, T.J., Lakshmi, V., Chan, T.K., Nghiem, S.V., 2003. Soil moisture retrieval from AMSR-E. *IEEE Trans. Geosci. Remote Sens.* 41, 215–229.
- Njoku, E.G., Ashcroft, P., Chan, T.K., Li, L., 2005. Global survey of statistics of radio frequency interference in AMSR-E land observations. *IEEE Trans. Geosci. Remote Sens.* 43, 938–947.
- Okuyama, A., Imaoaka, K., 2015. Intercalibration of advanced microwave scanning radiometer-2. (AMSR2) brightness temperature. *IEEE Trans. Geosci. Remote Sens.* 53 (8), 4568–4577.
- Owe, M., De Jeu, R.A.M., Holmes, T.R.H., 2008. Multi-sensor historical climatology of satellite derived global land surface moisture. *J. Geophys. Res.: Atmos.* 113:F1 F01002. <http://dx.doi.org/10.1029/2007JF000769>.
- Parinussa, R.M., Holmes, T.R.H., Wanders, N., Dorigo, W.A., De Jeu, R.A.M., 2015. A preliminary study towards consistent soil moisture from AMSR2. *J. Hydrometeorol.* 16, 932–947.
- Peel, M.C., Finlayson, B.L., McMahon, T.A., 2007. Updated world map of the Köppen–Geiger climate classification. *Hydrol. Earth Syst. Sci.* 11, 1633–1644.
- Ray, R.L., Jacobs, J.M., Cosh, M.H., 2010. Landslide susceptibility mapping using down-scaled AMSR-E soil moisture: a case study from Cleveland Corral, California, US. *Remote Sens. Environ.* 114 (11), 2624–2636.
- Reichle, R.H., Koster, R.D., De Lannoy, G.J.M., Forman, B.A., Liu, Q., Mahanama, S.P.P., et al., 2011. Assessment and enhancement of MERRA land surface hydrology estimates. *J. Clim.* 24 (24), 6322–6338.
- Rienecker, M., Suarez, M.J., Gelaro, R., Todling, R., Bacmeister, J., Liu, E., et al., 2011. MERRA – NASA's modern-era retrospective analysis for research and applications. *J. Clim.* 24 (14), 3624–3648.
- Rossato, I., De Jeu, R.A.M., Alvala, R., Souza, S., 2011. Evaluation of soil moisture from satellite observations over south America. *Int. J. Remote Sens.* <http://dx.doi.org/10.1080/01431161.2010.532169>.
- Su, C.-H., Ryu, D., Western, A.W., Wagner, W., 2013a. De-noising of passive and active microwave satellite soil moisture time series. *Geophys. Res. Lett.* 40 (14), 3624–3630.
- Su, C.-H., Ryu, D., Young, R., Western, A., Wagner, W., 2013b. Intercomparison of microwave satellite soil moisture retrievals over the Murrumbidgee Basin, southeast Australia. *Remote Sens. Environ.* 134, 1–11.
- Su, C.-H., Ryu, D., Crow, W.T., Western, A.W., 2014a. Beyond triple collocation: applications to soil moisture monitoring. *J. Geophys. Res. Atmos.* 119 (11), 6419–6439.
- Su, C.-H., Ryu, D., Crow, W.T., Western, A.W., 2014b. Stand-alone error characterization of microwave satellite soil moisture using a Fourier method. *Remote Sens. Environ.* 154, 115–126.
- Su, C.-H., Narsey, S.Y., Gruber, A., Xaver, A., Chung, D., Ryu, D., Wagner, W., 2015. Evaluation of post-retrieval de-noising of active and passive microwave satellite soil moisture. *Remote Sens. Environ.* 163, 127–139.
- Schmugge, T.J., Kustas, W.P., Ritchie, J.C., Jackson, T.J., Rango, A., 2002. Remote sensing in hydrology. *Adv. Water Resour.* 25, 1367–1385.
- Turner, W., Spector, S., Gardiner, N., Fladeland, M., Sterling, E., Steininger, M., 2003. Remote sensing for biodiversity science and conservation. *Trends Ecol. Evol.* 18, 306–314.
- Wagner, W., Dorigo, W.A., de Jeu, R.A.M., Fernandez-Prieto, D., Benveniste, J., Haas, E., et al., 2012. Fusion of Active and Passive Microwave Observations to Create an Essential Climate Variable Data Record on Soil Moisture. XXII ISPRS Congress, Melbourne, Australia.
- Wanders, N., Karssenberg, D., de Roo, A., de Jong, S.M., Bierkens, M.F.P., 2014. The suitability of remotely sensed soil moisture for improving operational flood forecasting. *Hydrol. Earth Syst. Sci.* 18:2343–2357. <http://dx.doi.org/10.5194/hess-18-2343-2014>.
- Wang, J.R., Schmugge, T.J., 1980. Empirical model for the complex dielectric permittivity of soils as a function of water content. *IEEE Trans. Geosci. Remote Sens.* GE-18, 288–295.
- Yi, Y., Kimball, J.S., Jones, L.A., Reichle, R.H., McDonald, K.C., 2011. Evaluation of MERRA land surface estimates in preparation for the soil moisture active passive mission. *J. Clim.* 24, 3797–3816.
- Zeng, J., Li, Z., Chen, Q., Bi, H., Qiu, J., Zou, P., 2015. Evaluation of remotely sensed and re-analysis soil moisture products over the Tibetan plateau using in-situ observations. *Remote Sens. Environ.* 163, 91–110.